LBNL-……

Published in
Journal of Material Science, vol. 48, pp. 3789-3797, 2013.
Available on-line
http://dx.doi.org/10.1007/s10853-013-7179-y

Structural, optical, and electrical properties of indium doped cadmium oxide films prepared by pulsed filtered cathodic arc deposition

Yuankun Zhu [a, b], Rueben J. Mendelsberg [b,c], Jiaqi Zhu [a] *, Jiecai Han [a], and André Anders [b]

[a] *Harbin Institute of Technology, Harbin 150080, People's Republic of China*

[b] *Lawrence Berkeley National Laboratory, Plasma Applications Group, Berkeley, California, 94720*

[c] *Argonne National Laboratory, Materials Science Division, Argonne, Illinois, 60439*

Acknowledgements

The authors would like to thank K.M. Yu and S.H.N. Lim for their contributions to this work. Research was supported by the LDRD Program of Lawrence Berkeley National Laboratory, by the Assistant Secretary for Energy Efficiency and Renewable Energy, Office of Building Technology, of the U.S. Department of Energy under U.S. Department of Energy Contract No. DE-AC02-05CH11231. Additional support was provided by the National Natural Science Foundation of China (Grant No.51072039 and 51222205), and the Ph.D. Programs Foundation of the Ministry of Education of China (20112302110036).

* Corresponding author: Email: zhujq@hit.edu.cn (Jiaqi Zhu); Tel. / Fax: +86-451-86417970

ABSTRACT

Indium doped cadmium oxide (CdO:In) films were prepared on glass and sapphire substrates by pulsed filtered cathodic arc deposition (PFCAD). The effects of substrate temperature, oxygen pressure, and an MgO template layer on film properties were systematically studied. The MgO template layers significantly influence the microstructure and the electrical properties of CdO:In films, but show different effects on glass and sapphire substrates. Under optimized conditions on glass substrates, CdO:In films with thickness of about 125 nm showed low resistivity of 5.9×10^{-5} Ωcm, mobility of 112 cm^2/Vs, and transmittance over 80% (including the glass substrate) from 500-1500 nm. The optical bandgap of the films was found to be in the range of 2.7 to 3.2 eV using both the Tauc relation and the derivative of transmittance. The observed widening of the optical bandgap with increasing carrier concentration can be described well only by considering bandgap renormalization effects along with the Burstein–Moss shift for a nonparabolic conduction band.

Keywords: indium doped cadmium oxide, pulsed filtered cathodic arc deposition, transparent conducting oxides, bandgap shift

1. Introduction

Transparent conducting oxides (TCOs) including tin oxide (SnO_2), indium oxide (In_2O_3), zinc oxide (ZnO), and cadmium oxide (CdO) have attracted much attention due to their tremendous importance in optical and electrical applications [1-3]. Extensive efforts have been made to obtain high quality TCO films with high conductivity and transparency. CdO has exceptional electrical and optical properties, making it a promising material meeting the strict requirements of TCO applications demanding high performance. However, as it is known, the toxicity and the relatively narrow intrinsic bandgap of CdO limit its application. Fortunately, the bandgap of CdO can be considerably widened via the Burstein-Moss shift by increasing the electron concentration [4-6]. Therefore, dopants including indium (In), tin (Sn), titanium (Ti), zinc (Zn), aluminum (Al), yttrium (Y), and fluorine (F) have been introduced into CdO in order to improve the conductivity and widen the bandgap [4,6-12]. Aside from environmental issues, doped CdO materials are nearly ideal for photoelectrical and other possible applications, such as solar energy harvesting, optical communications, gas sensors, thin-film resistors, IR heat mirrors, etc. [3,7,13].

Among other effects, doping TCO films can induce a shift in the bandgap. In heavily doped n-type semiconductors, the shift is due to the competitive effects of the Burstein–Moss (BM) band filling and the fundamental bandgap narrowing (BGN) [14-16]. Narrowing of the fundamental gap is the result of many-body effects and is also known as bandgap renormalization [17,18]. Good agreement between theory and experiment for the bandgap shift of heavily doped group IV, III-V, and II-VI semiconductors has been demonstrated [14,18,19]. For pure CdO films, the bandgap shift has been extensively studied using the Burstein–Moss (BM) theory while accounting for the many-body effects [20,21]. However, for heavily doped CdO, there has not yet been a systematic report on the dopant-induced bandgap shift which also accounts for the nonparabolicity of the conduction band. All the previous investigations seem to leave out the nonparabolicity or ignore the bandgap renormalization [13,22-28]. For a complete understanding of the bandgap shift in doped CdO, an effective theoretical model is needed which considers BGN and a nonparabolic BM shift simultaneously.

In this work, CdO:In films were grown on glass and sapphire substrates by pulsed filtered cathodic arc deposition (PFCAD). PFCAD is a lesser known technique but it has been utilized to grow high quality aluminum doped zinc oxide (AZO) films [29]. Excellent CdO:In films can also be obtained by the natural advantages of PFCAD [10,30]. Previous studies have shown that the crystallinity and the electrical properties of CdO films are strongly dependent on the growth conditions and the crystalline orientations of substrate materials as well as template layers [7,31]. Therefore, the effects of MgO template layers and substrate materials on film structural, electrical, and optical properties were also studied. Furthermore, the dependence of the bandgap shift on carrier concentration was carefully measured and systematically investigated by considering the nonparabolic conduction band and the different many-body effects.

2. Experiment

CdO:In films were grown on borosilicate glass and sapphire substrates by PFCAD using a similar setup of growth system described in ref 10. Metallic cadmium (99.99% purity) and indium (99.99% purity) rods were used as two separate source cathodes which were alternately pulsed. The cadmium and indium plasmas passed through a 90°-bend open coil electromagnetic filter to remove most of the macroparticles. Electrical plasma-generating pulses of 1 ms duration with a peak amplitude of 780 A were delivered at 1 Hz by a pulse-forming network [32]. The concentration of indium in the films was controlled by adjusting the relative number of pulses on each of the two cathodes. Unless otherwise stated, all of the CdO:In films in this study were grown using 30 pulses of cadmium for every 1 pulse of indium, resulting in an indium content of about 2.2±0.7 at.% measured by energy-dispersive X-ray spectroscopy (EDS). The detailed growth process has been described in our previous work [33]. To investigate the effect of substrate materials on film properties, 50 nm and 100 nm thick MgO template layers were pre-grown on glass and sapphire substrates by PFCAD at 425 °C. The growth parameters are listed in Table 1.

Film thickness was measured using step profilometry with accuracy of about 10 nm. Film structure was investigated by a Bruker X-ray diffractometer (XRD) equipped with an area detector or a Phillips X' Pert-Pro X-ray diffractometer depending on availability. For the Bruker, a LaB_6 powder diffraction standard was used to ensure calibration of the 2θ angle and to measure the significant instrumental broadening of the area detector. Surface morphology was studied by atomic force microscopy (AFM, Veeco MultiMode). Optical transmittance and reflectance from 250-2500 nm were measured using a Perkin Elmer Lambda 950 dual beam photo-spectrometer. The electrical properties were characterized by Hall measurements in the Van der Pauw geometry using an Ecopia HMS-3000 system.

3. Results and discussion

3.1 Structural properties

Atomic force micrographs of 460 nm thick CdO:In films prepared on different substrates are shown in Fig. 1 with the surface roughness listed in Table 1. The pre-grown MgO template layers are very smooth and show mean surface roughness less than 0.8 nm, which is probably due to the small thickness. Continuously packed and uniform features are observed in all of the CdO:In films. The CdO:In films on glass are smooth with root-mean-square roughness (*Rq*) of 3.2 nm over a 1μm×1μm area, while the CdO:In films on MgO/glass are somewhat rougher, exhibiting *Rq* of 6.8 nm. Increased

roughness due to the MgO template is also observed for CdO:In films deposited on sapphire, implying that the MgO layer has an important influence over the CdO:In microstructure.

The XRD patterns of CdO:In films deposited on glass at various oxygen pressures are shown in Fig. 2(a). All of the as-deposited films appear phase-pure and are polycrystalline, with an fcc structure typical of CdO (PDF card No: 005-0640). No extra peaks of In, In_2O_3 and/or Cd_2InO_4 due to the addition of indium in CdO films are observed, indicating that most of the In substitutes for the Cd or is incorporated interstitially instead of forming a new phase. With increasing oxygen pressure, the intensity of the (200) peak increases, while that of the (220) and (111) peaks decrease as shown in Fig. 2(b). The crystallite size calculated from the Scherrer equation is about 35-45 nm and is almost constant with increasing oxygen pressure.

The variation of crystallite alignment with oxygen partial pressure is likely related to the effect of the oxygen vacancy content on the diffusion rate of Cd and O atoms [24,34]. At relatively high oxygen pressure, it is expected that the diffusion rate of cadmium and oxygen decreases since less oxygen vacancies are able to provide sites for atom migration. Therefore, adatoms more easily find their correct lattice sites and the (200) direction with the lowest surface energy and highest packing density becomes the preferred orientation. Similar phenomena are also observed in ITO films grown at different oxygen pressures [34].

Similar to the effects of oxygen pressure, variation of the preferential orientation is observed with increasing substrate temperature as shown in Fig. 3. Several reflections can be observed when the films are deposited at low temperature, but when the substrate is pre-heated to 425 °C, only the (200) peak is present. The full-width at half-maximum (FWHM) of the (200) peak decreases with increasing substrate temperature and the crystallite size is listed in Table 1. Furthermore, a sharp peak in the χ-direction for the (200) reflection is observed for the films grown at 425 °C, while broad and nearly flat χ-scans are obtained for films deposited at lower temperatures. Thus, the overall crystal quality and the crystallite alignment perpendicular to the substrate are remarkably improved with increasing substrate temperature.

Fig. 4 shows the XRD patterns of CdO:In films prepared at 425 °C on glass and sapphire, both with and without a pulsed arc-grown MgO buffer layer. On glass substrates, the films show a strong (200) peak. However, introducing an MgO template layer changes the growth directions, which leads to diverse preferential orientations. When deposited on sapphire substrates, a broad low-intensity hump (200) peak is observed indicating the CdO:In films are likely X-ray amorphous. However, with a 50 nm MgO template layer on sapphire substrate, a single, strong (200) peak of CdO:In films is observed. It is interesting that the XRD spectra of the pulsed arc-grown CdO films on sapphire are remarkably different from the spectra of PLD grown films, where only the latter show an intense (200) peak. [21,28]. This difference is not yet understood and is, perhaps, surprising since laser ablation and cathodic arcs produce ions of similar energies.

Our observations show that the MgO template layers change the CdO:In growth direction on glass substrates and apparently improve the crystalline quality on sapphire substrates. These different effects of MgO template layers on CdO:In structure are likely associated with the different structures of MgO

layers grown on glass and sapphire substrates. The MgO layers on glass substrates show two weak XRD peaks assigned to the (200) and (220) planes of cubic MgO. However, on sapphire substrates, the template layer shows three weak peaks corresponding to the (220), (400), and (440) reflections of fcc $MgAl_2O_4$ (Fig. 5), indicating significant Al diffusion into the deposited MgO layer. It is perhaps surprising that the crystal properties of CdO:In films on MgO/sapphire ($MgAl_2O_4$) substrates are significantly improved since the $MgAl_2O_4$ buffer layers show about a 40% lattice mismatch with the CdO:In films. Further work directly probing the interface layers is needed to fully understand the structure of these samples.

3.2 Electrical properties

Fig. 6 shows the electrical properties of CdO:In films as a function of oxygen pressure. The Hall mobility substantially increases while the carrier concentration slightly decreases with increasing oxygen pressure, resulting in a nearly constant resistivity. The variation of carrier concentrations is attributed to the decrease of oxygen vacancies serving as donors, which is consistent with the aforementioned XRD study. Thus, the ionized impurity scattering decreases, which is important since it is a main scattering mechanism that limits the mobility in heavily doped semiconductors. Consequently, the mobility substantially increases with increasing oxygen pressure.

Electrical properties of CdO:In films as a function of substrate temperature are shown in Fig. 7. As the deposition temperature increases, arriving adatoms achieve a greater surface mobility, allowing them to thermalize at more favorable positions on the growing film surface [35]. This produces larger crystallites (shown in Table 1) with reduced intragrain defect density, both of which facilitate higher electron mobility. In addition, the improvement in the alignment of crystallites further increases the electron mobility and reduces the resistivity.

The electrical properties of CdO:In films prepared on different substrates at 425 °C are listed in Table 1. On glass substrates, the 100 nm MgO template layers lower the resistivity and improve the mobility. On sapphire substrates, higher resistivity and lower mobility are observed in the CdO:In films with MgO template layers. This phenomenon is also observed at lower substrate temperatures. However, both of these observations are not consistent with the XRD, which shows the MgO template layer improved the crystal quality of samples deposited on sapphire while deteriorating the crystal quality for those deposited on glass. Clearly, a more detailed study into the interface structure and carrier scattering mechanisms is needed.

3.3 Optical properties

The transmittance and reflectance of CdO:In/glass stacks with film thickness about 230 nm are presented in Fig. 8. Average transmittance is greater than 80% from 500 to about 1300 nm in all of the CdO:In films. Over the range studied in this work, the oxygen pressure has virtually no effect on film transparency in the visible region. However, in the near infrared range, the CdO:In films grown at 3 mTorr show slightly blue shift of the plasma edge compared to the other films. This results from the slightly higher carrier concentration of the films grown at 3 mTorr.

Different from the influence of oxygen pressure, the transmittance and reflectance of CdO:In/glass stacks prepared at various substrate temperatures vary significantly as shown in Fig. 9. The CdO:In

films show mean transmittance over 80% in the 500-1500 nm wavelength range, except for the one grown at room temperature. The ultraviolet (UV) absorption edge as well as the NIR plasma edge shifts with changing growth temperature. This is a result of the variation of carrier concentration which shifts the bandgap absorption via the Burstein-Moss effect while the free carrier absorption and reflection influences the near infrared. In addition, the MgO template layer negligibly influences the transmittance and reflectance, which is likely due to the MgO template layer being extremely transparent and very smooth.

The optical bandgap (E_g) of CdO:In films is derived from the optical transmittance spectrum. The absorption coefficient (α) is calculated using the equation [36]:

$$\alpha = -\frac{1}{d}\ln[\frac{T}{(1-R)^2}] \quad (1)$$

where T is the transmittance, R is the reflectance, and d is the film thickness, respectively. According to the Tauc relation, the absorption coefficient (α) and the incident photon energy ($h\upsilon$) are related by [27]:

$$(\alpha h\upsilon)^2 = A(h\upsilon - E_g) \quad (2)$$

where $h\upsilon$ and A are the photon energy and a constant, respectively. The direct optical bandgap of CdO:In thin films is shown in Fig. 10. It should be mentioned that the calculated optical bandgap is about 0.02-0.05 eV smaller than that in Fig. 10 when the reflectance was neglected (i.e. R=0) in equation (1).

It is extremely important to note that the Tauc relation assumes a parabolic conduction band. However, in our previous study, nonparabolicity of the conduction band in heavily doped arc-grown CdO films was clearly observed [37]. Therefore, the bandgap of CdO:In films is also calculated using the derivative of the transmittance spectra [38,39].

$$E_g^T = \frac{hc}{\lambda_{\max}} \quad (3)$$

where h is the Planck constant, c is the light velocity, and $\lambda_{\max}$ is the wavelength of the maximum derivative of the high energy portion of the transmittance spectra, well away from the interference fringes. The results (E_g^T) reveal very similar dependence on carrier concentration as the Tauc relation, as shown in Fig. 10(b). Despite the spread in the growth conditions, the optical bandgap clearly widens with increasing carrier concentration.

In previous studies, the optical bandgap was obtained from the derivative of the absorption coefficient measured by photoacoustic spectroscopy [38]. In Fig. 10(c), it is shown that taking the bandgap obtained from the derivative of the absorption coefficient calculated by equation (1) agrees very well with that derived from the transmittance alone. Furthermore, Fig. 10(c) shows that film thickness does not make much difference to the measured bandgap value for films showing similar carrier concentrations when using the Tauc or derivative methods.

It is noted that, in Fig. 10(b) and 10(c), the derivative-based bandgap measurements of the CdO:In films, despite the different growth conditions, are typically about 0.1-0.3 eV lower than those obtained from the Tauc plot. To study this deviation, the optical spectra of over 30 samples with different carrier concentrations and film thicknesses were carefully measured and similar results were observed. However, Segura et al. showed that using the Tauc relation gave lower bandgaps compared with that derived from the absorption coefficient in undoped CdO [28]. Similar results were also observed in single crystal PbI_2 by Ferreira da Silva at al [38]. The opposite results we obtain here imply that the difference between the Tauc and derivative bandgap measurements depends on the material system. Indium doping has a profound influence on the CdO band structure [6], which is likely the reason for the discrepancy between our work and that of Segura et al. [28]. Clearly, more work is needed to better understand the consequences of using the Tauc relation or other methods when using transmittance (absorbance) to determine the optical bandgap in any semiconductor.

3.4 Bandgap shift

Remarkable widening of the optical bandgap has been observed with increasing carrier concentration as shown in Fig. 10(b). The optical bandgap of a heavily doped n-type semiconductor is [15,40]:

$$E_g = E_{g0} + \Delta E_g^{BM} - \Delta E^{BGN} \tag{4}$$

where E_{g0}, ΔE_g^{BM}, ΔE^{BGN} are the fundamental bandgap of the undoped semiconductor, the Burstein-Moss shift, and the bandgap renormalization, respectively. In this work, E_{g0} for undoped CdO is assumed to be about 2.16 eV [20], and the bandgap widening at high carrier concentrations in corresponding CdO:In films are referred to this value.

According to Pisarkiewicz's model for nonparabolic conduction bands, the Burstein-Moss shift of the bandgap in a heavily doped n-type semiconductor is [22]:

$$\Delta E_g^{BM} = \frac{1}{2D}\left[\sqrt{1+2D\frac{\hbar^2}{m_0^*}(3\pi^2 n)^{2/3}} - 1\right] \tag{5}$$

where D is the nonparabolicity factor and m_0^* is the effective mass at the bottom of the conduction band. For pulsed arc-grown CdO films, D and m_0^* are found to be about 0.5 eV^{-1} and 0.17 m_e (m_e is the free electron mass) respectively, by analyzing the evolution of plasma energy with carrier concentration using the Drude theory [37]. The obtained m_0^* is consistent with Coutts' and Dou's results showing a value of about 0.14 m_e [26,41].

Competing with the BM shift is the bandgap renormalization, a many-body effect which is the result of electron-dopant interactions along with the Coulomb and exchange interactions between the conduction band electrons [15,26,40]. Based on Jain's model, in a heavily doped semiconductor, the bandgap renormalization can be described by [14,42]:

$$\frac{\Delta E^{BGN}}{R} = \frac{1.83}{r_s}\frac{\Lambda}{N_b^{1/3}} + \frac{0.95}{r_s^{3/4}} + \frac{\pi}{2}\frac{1}{r_s^{3/4}N_b}\left(1+\frac{m^*_{\min}}{m^*_{maj}}\right) \quad (6)$$

where R is the effective Rydberg energy for a carrier bound to a dopant atom, N_b is the number of equivalent band extrema, and Λ is the correction factor that accounts for anisotropy of the bands in n-type semiconductors and interaction between the heavy- and light-hole bands in p-type semiconductors. m^*_{maj} and $m^*_{\min}$ are majority- and minority-carrier density-of-state effective masses, respectively. $r_s = \left(\frac{3}{4\pi n}\right)^{1/3} \Big/ a^*$ is the average distance between majority carriers, normalized to the effective Bohr radius. For CdO, m^*_{maj} and $m^*_{\min}$ are m_e and $3\,m_e$, respectively [21,22,37], the relative dielectric constant is 21.9 [43], and the values of Λ and N_b are 1 [42]. The three terms in equation (6) represent the exchange energy of the majority carriers, the correlation energy, and the impurity interaction energy, respectively. Equation (6) has been demonstrated to be valid for AZO, ITO and other IV, III–V, and II–VI semiconductors [14,18,19,42].

Fig. 11 shows the comparison of the theoretical and experimental results of bandgap shift in CdO films as a function of carrier concentration. It is shown that the calculated bandgap shift agrees well with E_g^T and demonstrates that the Tauc relation overestimates the bandgap in these arc-grown CdO samples. Therefore, the bandgap of CdO can be well described by accounting for the nonparabolicity of the conduction band along with the bandgap renormalization. The nonparabolic Burstein-Moss shift is about 0.5-1.4 eV depending on the carrier concentration. Accordingly, the bandgap renormalization is typically around 0.2-0.4 eV.

For comparison, the Burstein-Moss shift assuming a parabolic conduction band and effective mass of $0.21\,m_e$ (See Ref. [20]) is shown in Fig. 11 and largely overestimates the bandgap widening. Better agreement with the observed shift can be obtained simply by adding in terms for bandgap renormalization. Remarkable improvement can be made by accounting for the nonparabolicity of the conduction band.

4. Conclusions

Highly transparent and conductive CdO:In films were prepared on glass and sapphire substrates by PFCAD. The structural, electrical, and optical properties of CdO:In films are strongly dependent on oxygen pressure, substrate temperature as well as MgO template layers. The MgO template layers significantly influence the microstructure and the electrical properties of CdO:In films, but show different effects on glass and sapphire substrates. Under optimized conditions on glass substrates, CdO:In films with thickness of about 125 nm show low resistivity of 5.9×10^{-5} Ωcm, mobility of 112 cm^2/Vs, and transmittance over 80% (including the glass substrates) from 500-1500 nm. The bandgap widening of CdO:In films can be well described by accounting for the combination of bandgap renormalization and Burstein–Moss effects considering the nonparabolicity of the conduction band. A simple expression for bandgap narrowing effects proposed for heavily doped n-type IV, III–V, and II–

VI semiconductors is successfully used to study the different effects on bandgap shift for CdO:In films. These pulsed arc-grown CdO:In films exhibiting high conductivity and transparency are potentially suitable for solar cells and other possible applications.

References

1. Lim JT, Jeong CH, Vozny A, Lee JH, Kim MS, Yeom GY (2007) Top-emitting organic light-emitting diode using transparent conducting indium oxide layer fabricated by a two-step ion beam-assisted deposition. Surf Coat Tech 201:5358-5362

2. Santos-Cruz J, Torres-Delgado G, Castanedo-Pérez R, Jiménez-Sandoval S, Márquez-Marín J, Zelaya-Angel O (2006) Au–Cu/p–CdTe/n–CdO/glass-type solar cells. Sol Energy Mater Sol Cells 90:2272-2279

3. Anna Selvan JA, Delahoy AE, Guo S, Li Y-M (2006) A new light trapping TCO for nc-Si:H solar cells. Sol Energy Mater Sol Cells 90:3371-3376

4. Wang A (2001) Indium-cadmium-oxide films having exceptional electrical conductivity and optical transparency: Clues for optimizing transparent conductors. Proc Natl Acad Sci 98:7113-7116

5. Ueda N, Maeda H, Hosono H, Kawazoe H (1998) Band-gap widening of CdO thin films. J Appl Phys 84:6174-6177

6. Jin S, Yang Y, Medvedeva JE, Wang L, Li S, Cortes N, Ireland JR, Metz AW, Ni J, Hersam MC, Freeman AJ, Marks TJ (2008) Tuning the properties of transparent oxide conductors dopant ion size and electronic structure effects on CdO-based transparent conducting oxides Ga- and In-doped CdO thin films grown by MOCVD. Chem Mater 20:220-230

7. Yan M, Lane M, Kannewurf CR, Chang RPH (2001) Highly conductive epitaxial CdO thin films prepared by pulsed laser deposition. Appl Phys Lett 78:2342-2344

8. Gupta RK, Ghosh K, Patel R, Kahol PK (2009) Highly conducting and transparent Ti-doped CdO films by pulsed laser deposition. Appl Surf Sci 255:6252-6255

9. Freeman AJ, Poeppelmeier KR, Mason TO, Chang RPH, Marks TJ (2000) Chemical and thin-film strategies for new transparent conducting oxides. MRS Bull 25:45-51

10. Zhu Y, Mendelsberg RJ, Zhu J, Han J, Anders A (2012) Transparent and conductive indium doped cadmium oxide thin films prepared by pulsed filtered cathodic arc deposition. Appl Surf Sci (In Press)

11. Dakhel AA (2011) Structural, optical and electrical measurements on boron-doped CdO thin films. J Mater Sci 46:6925-6931

12. Ismail RA, Rasheed BG, Salm ET, Al-Hadethy M (2007) High transmittance–low resistivity cadmium oxide films grown by reactive pulsed laser deposition. J Mater Sci 18:1027-1030

13. Dakhel AA (2009) Bandgap narrowing in CdO doped with europium. Opt Mater 31:691-695

14. Jain SC, McGregor JM, Roulston DJ (1990) Band-gap narrowing in novel III-V semiconductors. J Appl Phys 68:3747

15. Hamberg I, Granqvist CG, Berggren KF, Sernelius BE, Engström L (1984) Band-gap widening in heavily Sn-doped In_2O_3. Phys Rev B 30:3240-3249

16. Burstein E (1954) Anomalous optical absorption limit in InSb. Phys Rev 93:632-633

17. Berggren K, Sernelius B (1981) Band-gap narrowing in heavily doped many-valley semiconductors. Phys Rev B 24:1971-1986

18. Lu JG, Fujita S, Kawaharamura T, Nishinaka H, Kamada Y, Ohshima T, Ye ZZ, Zeng YJ, Zhang YZ, Zhu LP, He HP, Zhao BH (2007) Carrier concentration dependence of band gap shift in n-type ZnO:Al films. J Appl Phys 101:083705

19. Kim CE, Moon P, Kim S, Myoung JM, Jang HW, Bang J, Yun I (2010) Effect of carrier concentration on optical bandgap shift in ZnO:Ga thin films. Thin Solid Films 518:6304-6307

20. Jefferson PH, Hatfield SA, Veal TD, King PDC, McConville CF, Zúñiga–Pérez J, Muñoz–Sanjosé V (2008) Bandgap and effective mass of epitaxial cadmium oxide. Appl Phys Lett 92:022101

21. Speaks DT, Mayer MA, Yu KM, Mao SS, Haller EE, Walukiewicz W (2010) Fermi level stabilization energy in cadmium oxide. J Appl Phys 107:113706
22. Pisarkiewicz T, Zakrewska K, Leja E (1989) Scattering of charge carriers in transparent and conducting thin oxide films with a non-parabolic conduction band. Thin Solid Films 174:217-223
23. Zhao Z, Morel DL, Ferekides CS (2002) Electrical and optical properties of tin-doped CdO films deposited by atmospheric metalorganic chemical vapor deposition. Thin Solid Films 413:203-211
24. Zheng BJ, Lian JS, Zhao L, Jiang Q (2010) Optical and electrical properties of In-doped CdO thin films fabricated by pulse laser deposition. Appl Surf Sci 256:2910-2914
25. Deokate RJ, Salunkhe SV, Agawane GL, Pawar BS, Pawar SM, Rajpure KY, Moholkar AV, Kim JH (2010) Structural, optical and electrical properties of chemically sprayed nanosized gallium doped CdO thin films. J Alloys Compd 496:357-363
26. Dou Y, Egdell RG, Walker T, Law DSL, Beamson G (1998) N-type doping in CdO ceramics a study by EELS and photoemission spectroscopy. Surf Sci 398:241-258
27. Saha B, Thapa R, Chattopadhyay K (2008) Bandgap widening in highly conducting CdO thin film by Ti incorporation through radio frequency magnetron sputtering technique. Solid State Commun 145:33-37
28. Segura A, Sánchez-Royo JF, García-Domene B, Almonacid G (2011) Current underestimation of the optical gap and Burstein-Moss shift in CdO thin films: A consequence of extended misuse of α^2-versus-hν plots. Appl Phys Lett 99:151907
29. Anders A, Lim SHN, Yu KM, Andersson J, Rosén J, McFarland M, Brown J (2010) High quality ZnO:Al transparent conducting oxide films synthesized by pulsed filtered cathodic arc deposition. Thin Solid Films 518:3313-3319
30. Goldsmith S (2006) Filtered vacuum arc deposition of undoped and doped ZnO thin films: Electrical, optical, and structural properties. Surf Coat Tech 201:3993-3999
31. Wang L, Yang Y, Jin S, Marks TJ (2006) MgO(100) template layer for CdO thin film growth: Strategies to enhance microstructural crystallinity and charge carrier mobility. Appl Phys Lett 88:162115
32. Anders A, MacGill RA, McVeigh TA (1999) Efficient, compact power supply for repetitively pulsed, "triggerless" cathodic arcs. Rev Sci Instrum 70:4532-4535
33. Mendelsberg RJ, Lim SHN, Zhu YK, Wallig J, Milliron DJ, Anders A (2011) Achieving high mobility ZnO:Al at very high growth rates by dc filtered cathodic arc deposition. J Phys D: Appl Phys 44:232003
34. Choi CG, No K, Lee WJ, Kim HG, Jung SO, Lee WJ, Kim WS, Kim SJ, Yoon C (1995) Effects of oxygen partial pressure on the microstructure and electrical properties of indium tin oxide film prepared by dc magnetron sputtering. Thin Solid Films 258:274-278
35. Li X, Yan Y, Mason A, Gessert TA, Coutts TJ (2001) High mobility CdO films and their dependence on structure. Electrochem Solid-State Lett 4:C66
36. Li X, Young DL, Moutinho H, Yan Y, Narayanswamy C, Gessert TA, Coutts TJ (2001) Properties of CdO thin films produced by chemical vapor deposition. Electrochem Solid-State Lett 4:C43-C46
37. Mendelsberg RJ, Zhu Y, Anders A (2012) Determining the nonparabolicity factor of the CdO conduction band using indium doping and the Drude theory. J Phys D: Appl Phys 45:425302
38. Ferreira da Silva A, Veissid N, An CY, Pepe I, Barros de Oliveira N, Batista da Silva AV (1996) Optical determination of the direct bandgap energy of lead iodide crystals. Appl Phys Lett 69:1930-1932

39. Veissid N, An CY, Ferreira da Silva A, Pinto de Souza JI (1999) Gap Energy Studied by Optical Transmittance in Lead Iodide Monocrystals Grown by Bridgman's Method. Materials Research 2:279-281
40. Sernelius BE, Berggren KF, Jin ZC, Hamberg I, Granqvist CG (1988) Band-gap tailoring of ZnO by means of heavy Al doping. Phys Rev B 37:10244-10248
41. Coutts TJ, Young DL, Li X (2000) Search for improved transparent conducting oxides: A fundamental investigation of CdO, Cd_2SnO_4, and Zn_2SnO_4. J Vac Sci Technol, A 18:2646-2660
42. Jain SC, Roulston DJ (1991) A simple expression for band gap narrowing (BGN) in heavily doped Si, Ge, GaAs and Ge_xSi_{1-x} strained layers. Solid-State Eletron 34:453-465
43. Finkenrath H, Von Ortenberg M (1967). Z Angew Phys 23:323-328

Table 1 Properties of CdO:In films prepared at different conditions. *d* is film thickness, *D* is crystallite size calculated from (200) peak

No.	Substrate	P	T	d	D	R_q	μ	ρ	n
		mT	°C	nm	nm	nm	cm^2/Vs	10^{-5} Ωcm	10^{20} cm^{-3}
1	Glass	3	230	230	43	1.20	108	8.4	6.95
2	Glass	4	230	220	44	1.36	112	8.6	6.53
3	Glass	5	230	230	36	1.60	116	7.9	6.83
4	Glass	6	230	220	41	1.54	118	8.2	6.44
5	Glass	7	230	230	42	1.89	121	8.6	6.04
6	Glass	7	25	150	23	0.81	49	12.8	9.96
7	Glass	7	230	135	43	1.06	101	9.1	6.76
8	Glass	7	425	125	100	0.96	112	5.9	9.43
9	Glass	7	425	460	—	3.25	126	5.5	9.08
10	50nm MgO/glass	7	425	460	—	6.57	121	5.0	10.03
11	100nm MgO/glass	7	425	460	—	9.46	142	5.2	8.45
12	Sapphire	7	425	460	—	4.73	122	6.5	7.96
13	50nm MgO/sapphire	7	425	460	—	7.04	107	7.8	7.54

Figure captions

Fig. 1 AFM images of CdO:In films prepared on different substrates at 425 °C. The thickness of the CdO:In films is about 460 nm. (a) Glass, (b) 50 nm MgO/glass, (c) Sapphire, (d) 50 nm MgO/sapphire

Fig. 2 (a) XRD patterns of ICO films as a function of oxygen pressure. (b) Relative intensity ratio of (200)/(220) and crystallite size calculated from the (200) peak

Fig. 3 XRD patterns of ICO thin films as a function of substrate temperature. Inset: the chi direction of (200) peak

Fig. 4 XRD patterns of CdO:In films prepared at 425°C on different substrates (a) glass, (b) 50 nm MgO/glass, (c) 100 nm MgO/glass, (d) sapphire, (e) 50 nm MgO/sapphire. The relative intensities of (a) and (e) are multiplied by 1/5

Fig. 5 XRD patterns of MgO template layers on glass and sapphire substrates. These MgO films were characterized using the Phillips X' Pert-Pro

Fig. 6 Electrical properties of CdO:In films on glass substrates as a function of oxygen pressure. The growth temperature was 230 °C. The typical film thickness is about 230 nm

Fig. 7 Electrical properties of CdO:In films as a function of substrate temperature. The growth oxygen pressure was about 7 mTorr and the typical film thickness is about 135nm

Fig. 8 (a) Transmittance and (b) reflectance of CdO:In/glass stacks as a function of oxygen pressure. The thickness of the CdO:In films is about 220-230 nm, and the glass substrate is 1 mm thick. Line: a-3mTorr, b-4mTorr, c-5 mTorr, d-6 mTorr, e-7 mTorr

Fig. 9 Transmittance and reflectance of CdO:In/glass stacks as a function of substrate temperature. The thickness of the CdO:In films is about 125-150 nm, and the glass substrate is 1 mm thick

Fig. 10 (a) Optical bandgap of CdO:In films prepared at different oxygen pressures. (b) Bandgap of CdO:In films as a function of carrier concentration. (c) Optical bandgap of CdO films obtained from different methods. A: three samples grown at the same condition showing similar carrier concentrations and film thicknesses (230 nm). B: four samples showing similar carrier concentrations but different thicknesses (135 nm, 230 nm, 250 nm, 640 nm).

Fig. 11 Bandgap shift of CdO:In films as a function of carrier concentration. The electrical and optical properties of CdO:In thin films with different indium contents (0~9 at.%) are described in ref.10

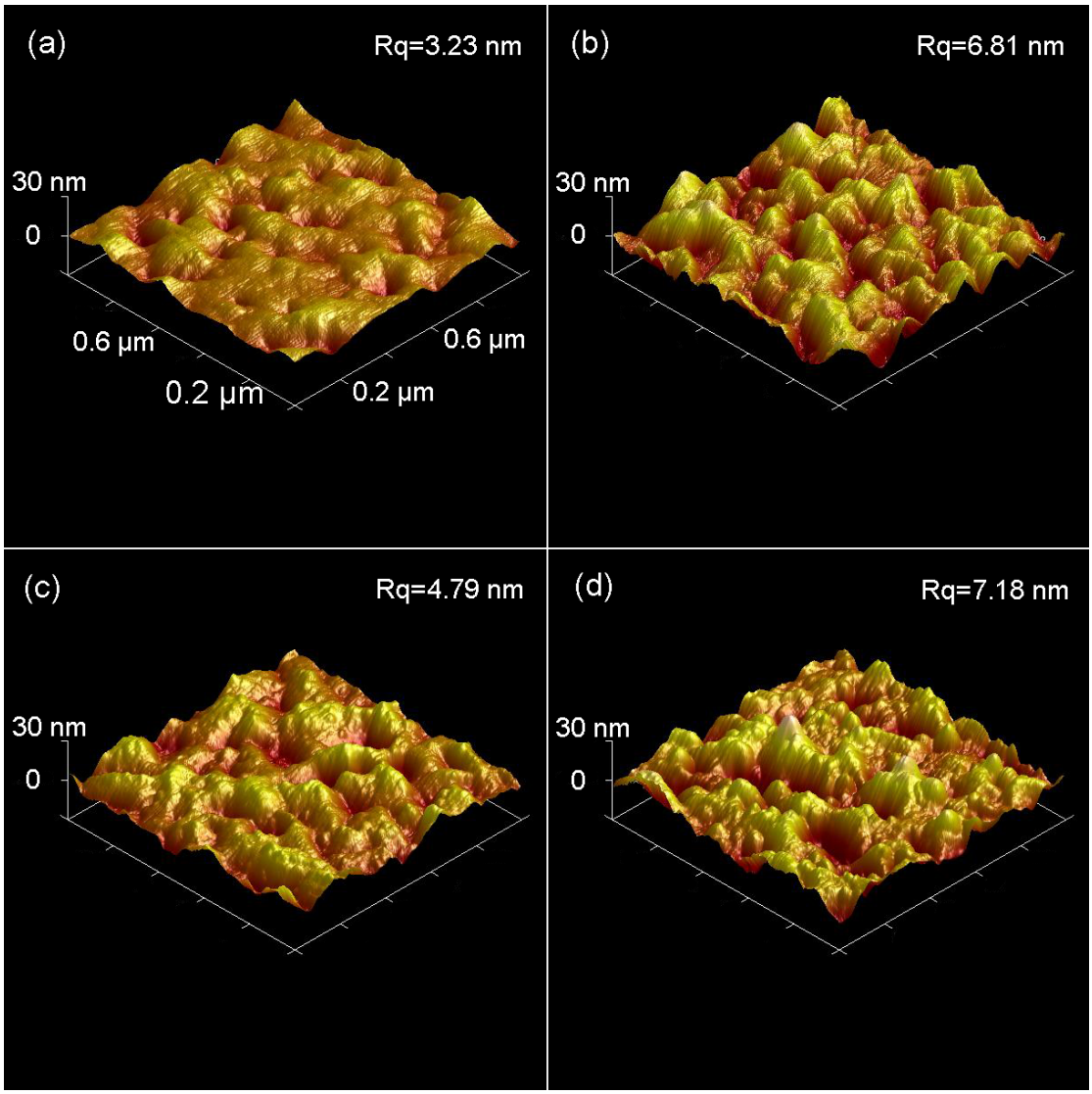
(a)
Rq=3.23 nm
30 nm
0
0.6 μm
0.2 μm
(b)
Rq=6.81 nm
30 nm
0
0.6 μm
0.2 μm
(c)
Rq=4.79 nm
30 nm
0
(d)
Rq=7.18 nm
30 nm
0

Fig. 1

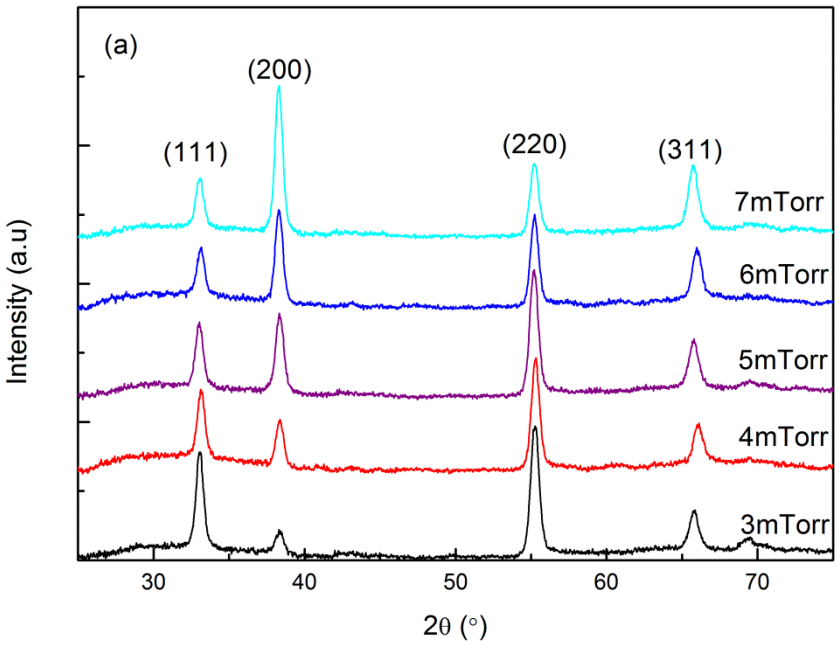
(a)
(200)
(111)
(220)
(311)
7mTorr
6mTorr
5mTorr
4mTorr
3mTorr
Intensity (a.u)
30
40
50
60
70
2θ (°)

Fig. 2a

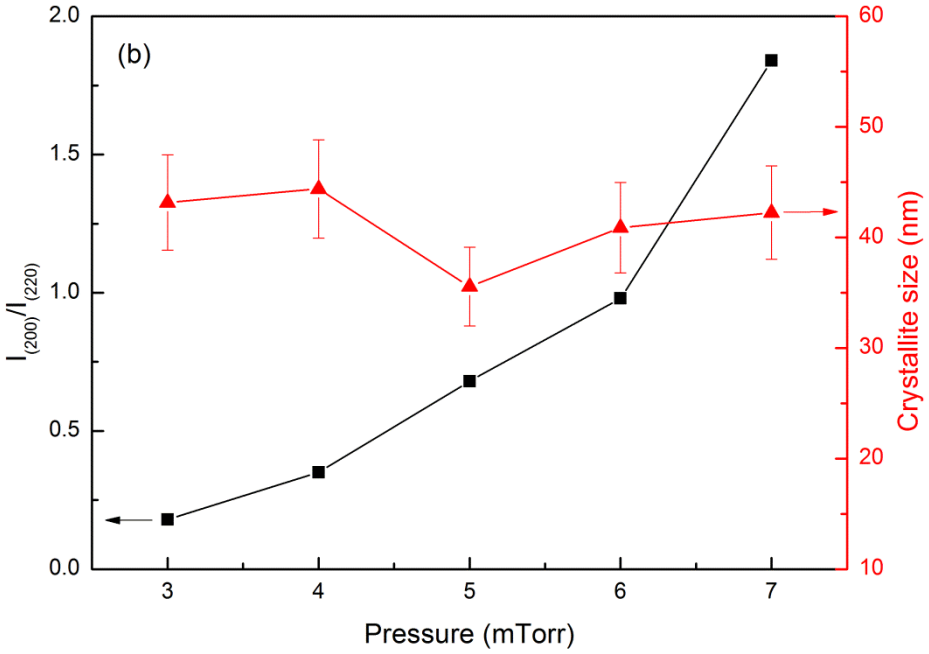
(b)
2.0
1.5
1.0
0.5
0.0
$I_{(200)}/I_{(220)}$
60
50
40
30
20
10
Crystallite size (nm)
3
4
5
6
7
Pressure (mTorr)

Fig. 2b

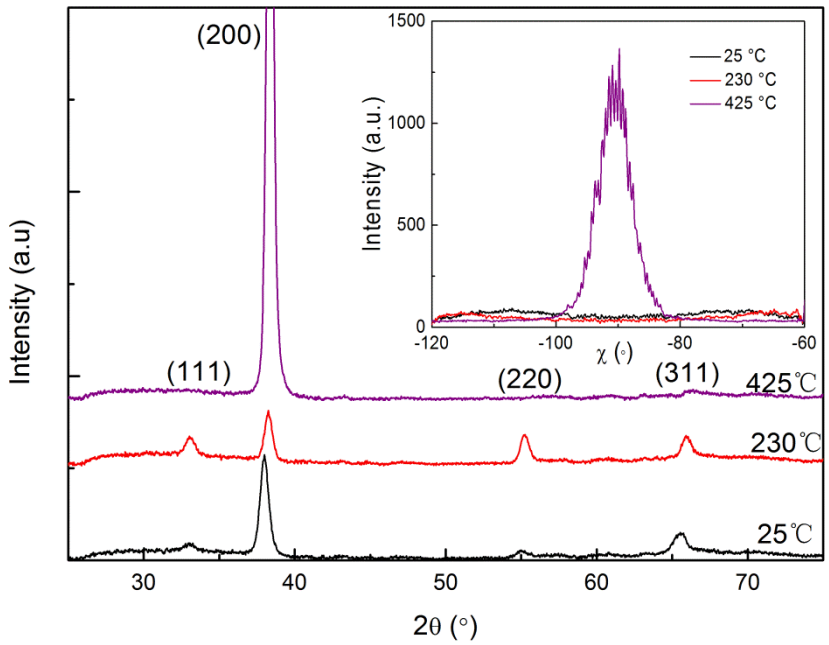
(200)
(111)
(220)
(311)
425℃
230℃
25℃
Intensity (a.u)
2θ (°)
30
40
50
60
70
Intensity (a.u.)
1500
1000
500
0
-120
-100
-80
-60
χ (°)
25 °C
230 °C
425 °C

Fig. 3

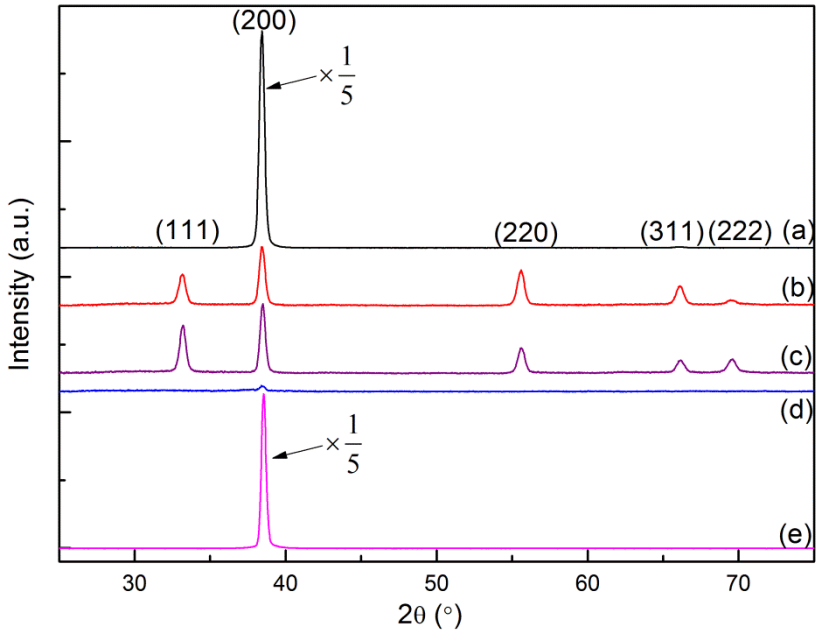

Fig. 4

Fig. 5

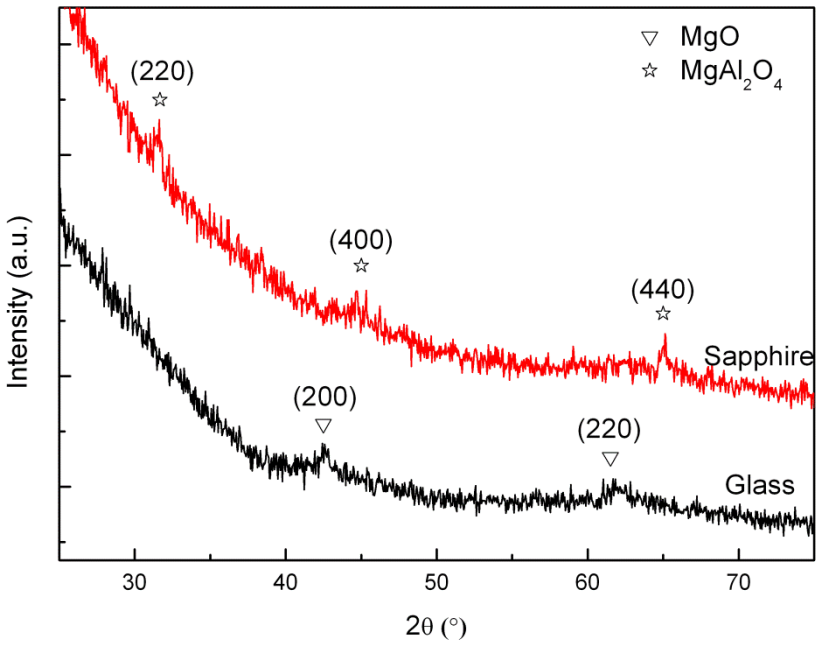
MgO
MgAl2O4
(220)
(400)
(440)
Sapphire
(200)
(220)
Glass
Intensity (a.u.)
30
40
50
60
70
2θ (°)

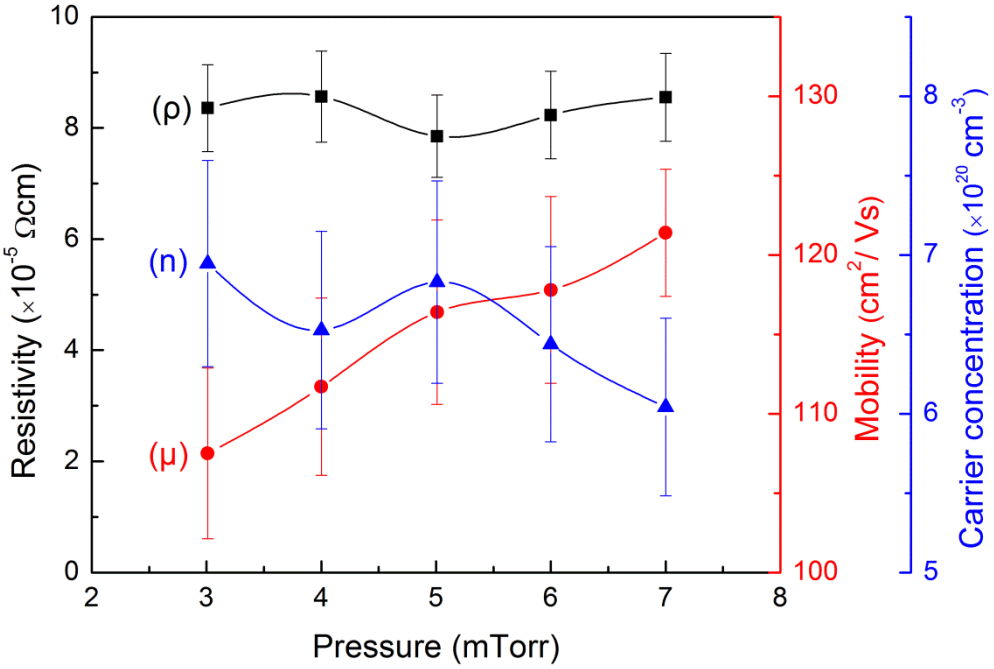
Resistivity (×10^-5 Ωcm)
Mobility (cm^2/ Vs)
Carrier concentration (×10^20 cm^-3)
Pressure (mTorr)
(ρ)
(n)
(μ)
10
8
6
4
2
0
130
120
110
100
8
7
6
5
2
3
4
5
6
7
8

Fig. 6

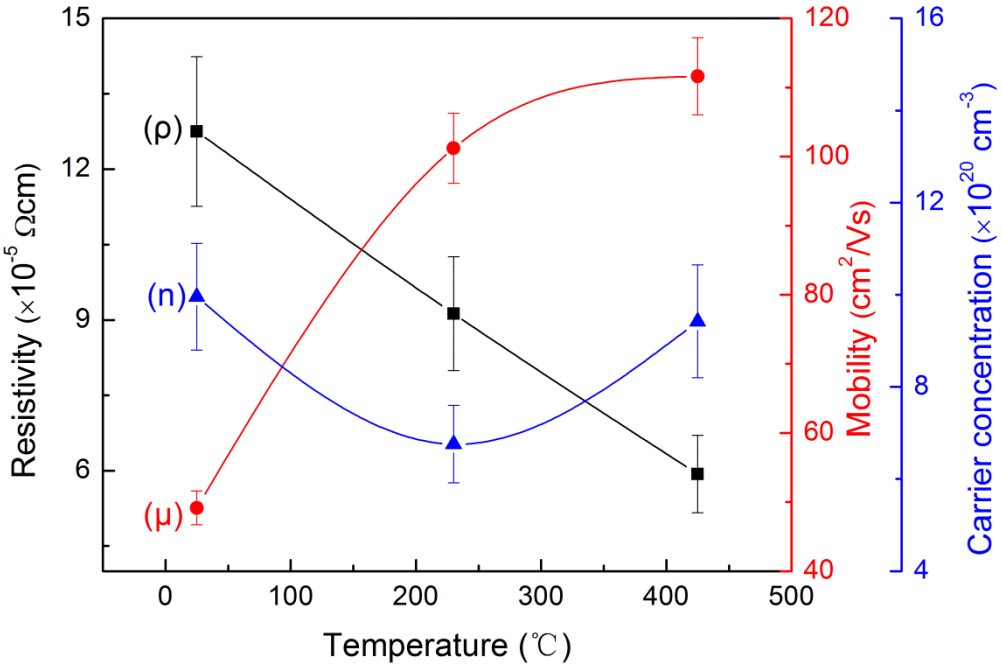
15
12
9
6
Resistivity (×10-5 Ωcm)
(ρ)
(n)
(μ)
120
100
80
60
40
Mobility (cm2/Vs)
16
12
8
4
Carrier concentration (×1020 cm-3)
0
100
200
300
400
500
Temperature (℃)

Fig. 7

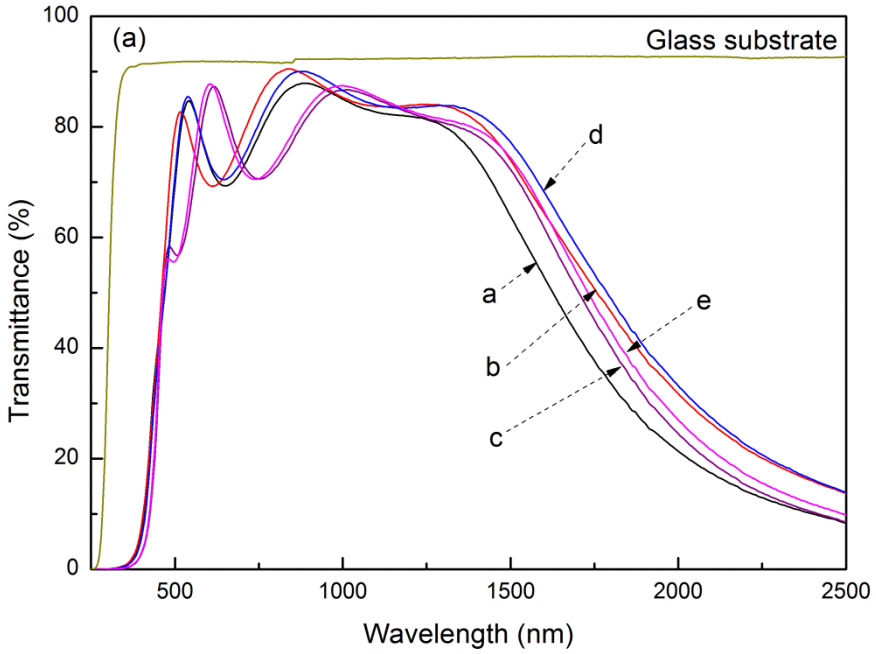
(a)
Glass substrate
Transmittance (%)
Wavelength (nm)
100
80
60
40
20
0
500
1000
1500
2000
2500
a
b
c
d
e

Fig. 8a

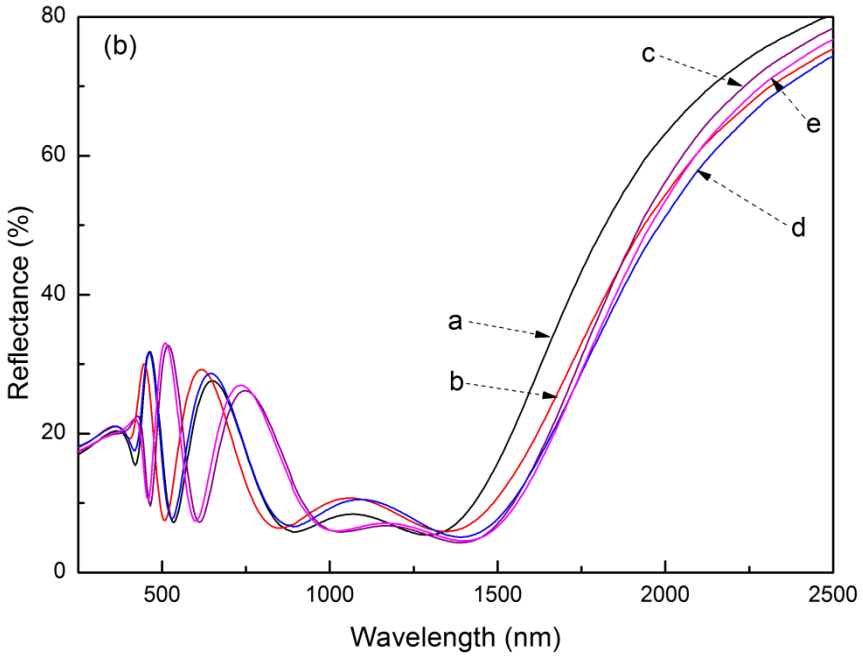
(b)
Reflectance (%)
Wavelength (nm)
0
20
40
60
80
500
1000
1500
2000
2500
a
b
c
d
e

Fig. 8b

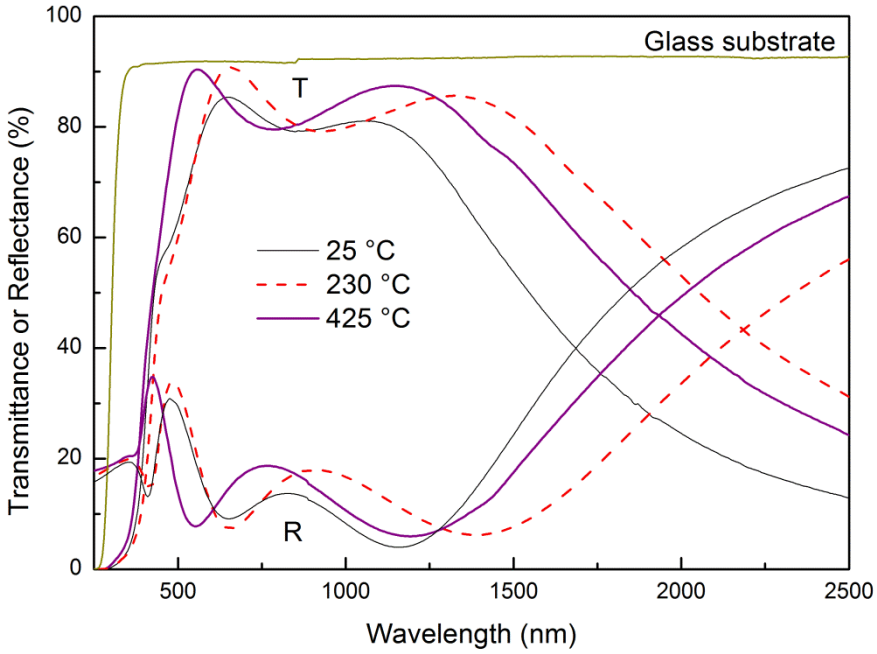
Glass substrate
T
R
25 °C
230 °C
425 °C
Transmittance or Reflectance (%)
Wavelength (nm)
0
20
40
60
80
100
500
1000
1500
2000
2500

Fig. 9

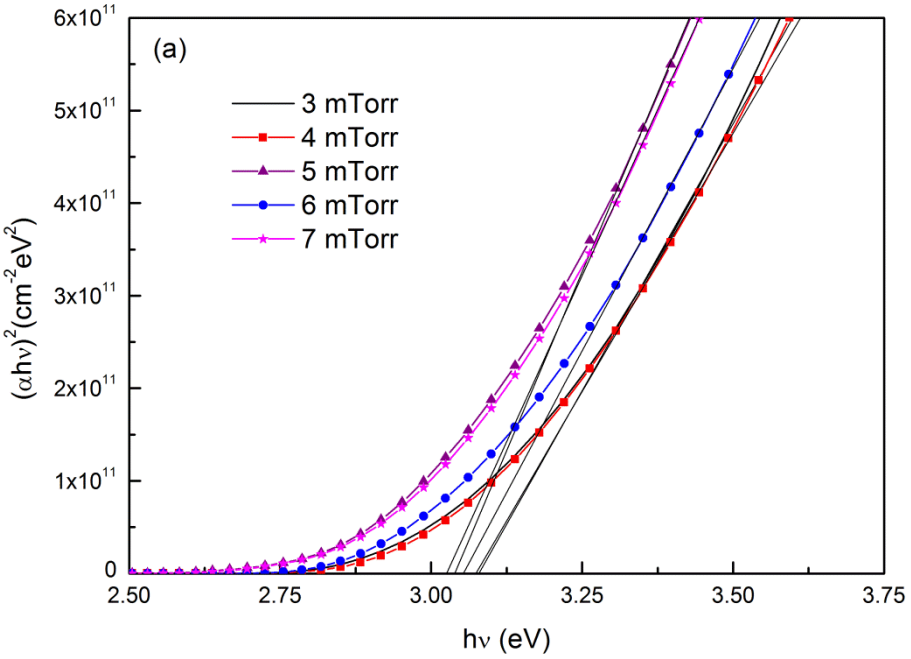
(a)
3 mTorr
4 mTorr
5 mTorr
6 mTorr
7 mTorr
6x10^11
5x10^11
4x10^11
3x10^11
2x10^11
1x10^11
0
(αhν)^2(cm^-2eV^2)
2.50
2.75
3.00
3.25
3.50
3.75
hν (eV)

Fig. 10a

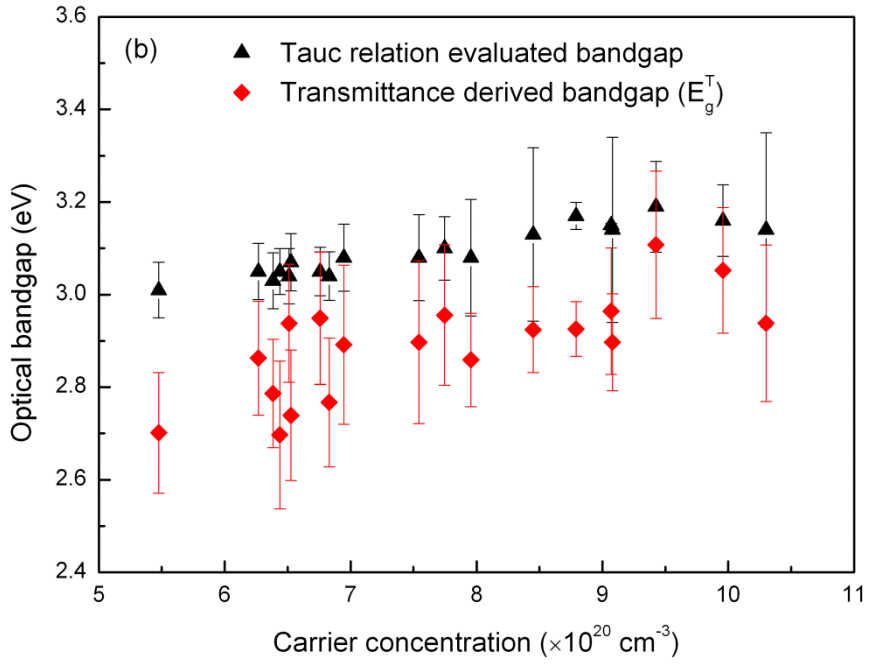
(b)
Tauc relation evaluated bandgap
Transmittance derived bandgap (E_g^T)
Optical bandgap (eV)
Carrier concentration (×10^{20} cm^{-3})
3.6
3.4
3.2
3.0
2.8
2.6
2.4
5
6
7
8
9
10
11

Fig. 10b

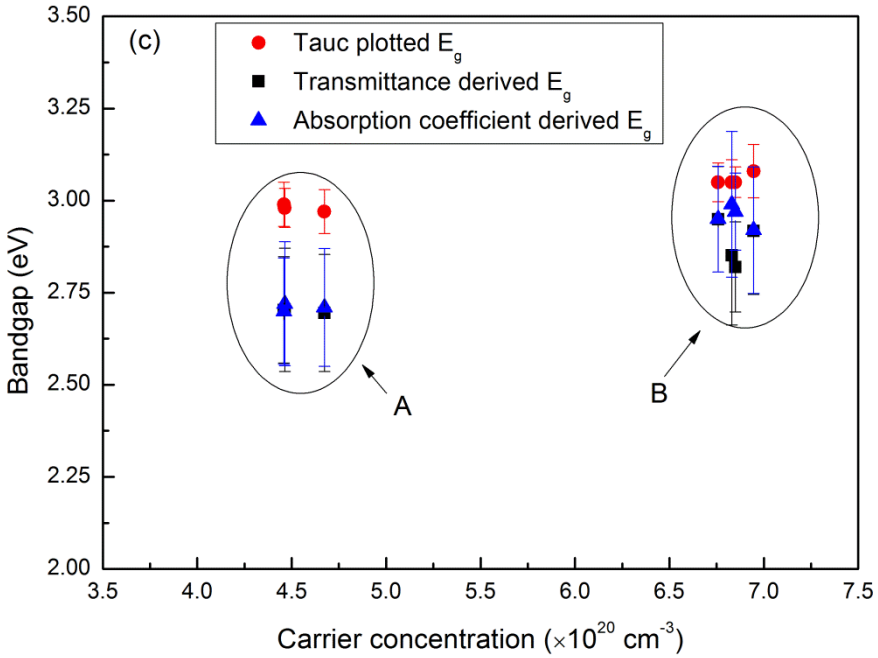
(c)
Tauc plotted E_g
Transmittance derived E_g
Absorption coefficient derived E_g
A
B
Bandgap (eV)
Carrier concentration (×10^20 cm^-3)
3.50
3.25
3.00
2.75
2.50
2.25
2.00
3.5
4.0
4.5
5.0
5.5
6.0
6.5
7.0
7.5

Fig. 10c

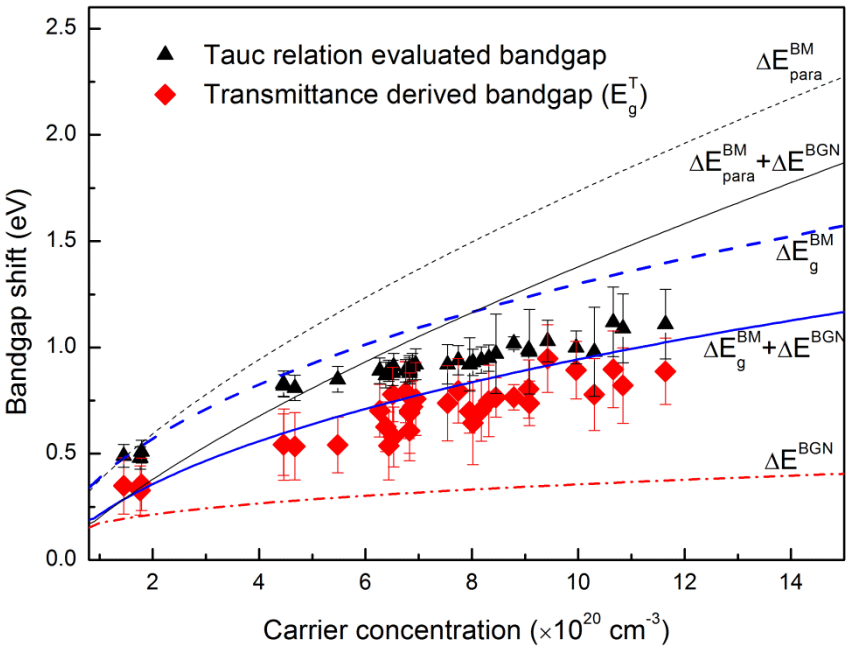
Tauc relation evaluated bandgap
Transmittance derived bandgap (E_g^T)
ΔE_{para}^{BM}
$\Delta E_{para}^{BM}+\Delta E^{BGN}$
ΔE_g^{BM}
$\Delta E_g^{BM}+\Delta E^{BGN}$
ΔE^{BGN}
Bandgap shift (eV)
Carrier concentration ($\times 10^{20}$ cm^{-3})
0.0
0.5
1.0
1.5
2.0
2.5
2
4
6
8
10
12
14

Fig. 11